Asian Journal of Chemistry; Vol. 25, No. 17 (2013), 9779-9784

ASIAN JOURNAL OF CHEMISTRY

http://dx.doi.org/10.14233/ajchem.2013.15321

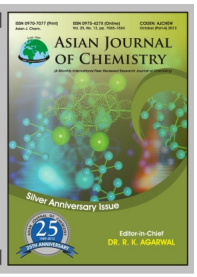

Fe_2O_3-SnO_2 Nanocomposite for Photocatalytic Oxidation of Nitric Oxide

E.S. BAEISSA

Department of Chemistry, Faculty of Science, King Abdulaziz University, P.O. Box 80203, Jeddah 21589, Saudi Arabia

Corresponding author: Fax: +966 2 6952292 Tel: +966 2 6400000; E-mail: elhambaeissa@gmail.com

(*Received*: 13 February 2013; *Accepted*: 23 October 2013) AJC-14274

A novel visible-light-activated Fe_2O_3-SnO_2 nanocomposite photocatalyst was prepared by co-precipitation method and characterized by X-ray diffraction, transmission electron microscopy, N_2 adsorption-desorption measurement and UV-visible diffuse reflectance spectroscopy. The results showed that a Fe_2O_3 and SnO_2 were present in the composites. The characterization results found that the phase composition, crystallite size, BET surface area and optical absorption of the samples varied significantly with the molar ratio of Sn to Fe. The Fe_2O_3-SnO_2 photocatalyst (the molar ratio of Fe to Sn is 2:1) calcined at 550 ºC for 5 h exhibited maximum photocatalytic activity because it has a smaller band gap and a higher surface area of 120 $m^2\ g^{-1}$. Under visible-light irradiation, the degradation efficiency of nitric oxide reached 95.0 %, which is *ca.* 1.72 times higher than that of the nanoparticles SnO_2 (Aldrich).

Key Words: Fe_2O_3-SnO_2 composites, Co-precipitation synthesis, Photocatalytic activity, Nitric oxide, Photocatalytic oxidation efficiency.

INTRODUCTION

Nitrogen oxides (NOx) exhausted from stationary sources and mobile sources can cause ozone depletion, photochemical smog and the acid deposition[1,2]. With the development of society and industry, increasing consumption of fossil fuels has resulted in large emissions of NOx. Among the NOx emitted from stationary combustion sources, more than 90 % of NOx is nitric oxide (NO). Wet scrubbing method, which is widely used for sulfur dioxide (SO_2) removal, promises to be less expensive than other methods for NOx removal, such as combustion modification, selective catalytic reduction (SCR) and selective noncatalytic reduction (SNCR)[3-6]. In order to remove NOx by wet scrubbing methods, it is necessary to oxidize NO to more soluble nitrogen dioxide (NO_2) or dinitrogen pentoxide (N_2O_5) in either gas or liquid phase[7,8].

Semiconductor photocatalysis, as one of the advanced physicochemical processes, was extensively studied for solving existing environmental problems such as wastewater treatment[9-14]. Among various oxide semiconductor photocatalysts, TiO_2 was intensively investigated because of its biological and chemical inertness, strong oxidizing power, nontoxicity and long-term stability[15,16]. However, there is still a problem that TiO_2 is effective only under ultraviolet irradiation ($\lambda < 380$ nm) due to its large band gap (3.2 eV)[17]. Furthermore, the fast recombination of photo-generated electron-hole pairs hinders the commercialization of this technology[18]. Therefore, it is of great interest to separate the electron-hole pairs effectively to increase the photon efficiencies and develop new visible-light photocatalysts to extend the absorption wavelength range into the visible-light region. In this sense, an interesting approach to deal with the issue is carried out by coupled semiconductor technique. Recently, there are a number of studies related to the photocatalytic activity of coupled semiconductor photocatalysts, such as TiO_2-CeO_2[19], WOx-TiO_2[20], ZnO/SnO_2[21], *etc*. These coupled semiconductor photocatalysts not only increase the photocatalytic efficiency, but also exhibit fine optical properties compared with the corresponding bulk ones due to the quantum confinement effects[22].

To the best of our knowledge, the visible-light-activated Fe_2O_3-SnO_2 nanocomposite photocatalyst for NO oxidation has not been reported. In this paper, we studied the effect of Fe/Sn molar ratio on photocatalytic activity of Fe_2O_3-SnO_2 photocatalysts for oxidation of nitric oxide under visible-light ($\lambda > 400$ nm) irradiation.

EXPERIMENTAL

Preparation of photocatalysts: The nanosized coupled Fe_2O_3-SnO_2 photocatalysts were prepared using the coprecipitation method. $SnCl_4 \cdot 5H_2O$ and $FeCl_3 \cdot 6H_2O$ (Analytical reagent grade, or A.R.) were used as the starting materials and ammonia (1:1) was used as the precipitator without further purification. $FeCl_3 \cdot 6H_2O$ and $SnCl_4 \cdot 5H_2O$ in the molar ratios of 3:1, 2:1, 1:1, 1:2 and 1: 3 were dissolved in a minimum amount of deionized water for the preparation of the coupled Fe_2O_3-SnO_2 photocatalysts with the Fe/Sn molar ratios of 3:1,

2:1, 1:1, 1:2 and 1: 3, labeled by Fe_3S_1, Fe_2S_1, Fe_1S_1, Fe_1S_2 and Fe_1S_3, respectively. The mixed solution was stirred at room temperature and added dropwise with the ammonia until it was completely precipitated. The precipitate was filtered and washed with deionized water until no Cl^- was found in the filtrates. Then the wet powder was dried at *ca.* 100 ºC in air to form the precursor of the Fe_2O_3-SnO_2 photocatalyst. Finally the precursors were calcined in air to prepare the nanosized photocatalysts. The nanosized Fe_2O_3 (Fe) and SnO_2 (S) were prepared using the same procedure as mentioned above except that the starting materials are $SnCl_4 \cdot 5H_2O$ for SnO_2 and $FeCl_3 \cdot 6H_2O$ for Fe_2O_3, respectively. For comparison, nanoparticles SnO_2 (Aldrich) was used without any further purification.

Characterization: The structure of the catalyst was examined by X-ray diffraction (XRD) on a Rigaku X-ray diffractometer system equipped with as RINT 2000 wide angle Joniometer using CuK_α radiation and a power of 40 kV × 30 mA. The intensity data were collected at 25 ºC over a 2θ range of 10-80º. The UV-VIS diffuse reflectance absorption spectra were recorded with a Shimadzu UV-2450 at 295 K. N_2-adsorption measurements was carried out at 77 K using Nova 2000 series, Chromatech. Prior to analysis, the samples were outgased at 250 ºC for 4 h. The morphology and particle size of the prepared samples were examined *via* a transmission electron microscope (Hitachi H-9500 operated at 300 kV).

Photo-oxidation of NO: All the photocatalytic activity experiments were carried out in a continuous setup. The setup consisted of a gas supply, reactor and analytical system. An air compressor, a NO cylinder (10,000 ppm, diluted by N_2) and a N_2 cylinder (99.9 %) were supplied as gas sources. By varying the flow rate of one stream air bubbled through a gas wash bottle, the humidity could be adjusted. The air, NO and N_2 streams were mixed to obtain the desired concentration (NO: 80-300 ppm, relative humidity: 75 %). The flow rate of the gas was 2 L/min and the space time was 10 s. Photocatalytic experiments were carried out in a 340 mL cylindrical Pyrex glass reactor. The immobilized catalyst was set into the reactor with a "Z" type. The photocatalyst was irradiated with a blue fluorescent lamp (150 W, S-3410, Sudo, maximum energy at 450 nm, designated as BFL hereafter) doubly covered with a UV cut filter and the UV intensity were confirmed to be under the detection limit (0.1 μW cm^{-2}) of a UV radiometer. The reaction temperature in the reactor was 80 ± 5 ºC, from the irradiation of the lamp. NO, NO_2 and O_2 were analyzed with a flue gas analyzer (Kane International Ltd., Model KM-9106). The relative humidity was measured with a relative humidity analyzer (Testo Co. Ltd., Model 605-H1). Blank tests were conducted with the Hg-arc turned on but without the photocatalyst using 80-300 ppm inlet NO, at 80 ± 5 ºC. The variation of the NO concentration could not be observed within 20 h irradiation. Furthermore, there was no change of the NO concentration when the Hg-arc lamp was turned off and the catalyst was present in the reactor.

The conversion % of NO is evaluated according to the following equation:

$$\text{NO conversion } (\%) = \frac{(NO_{inlet} - NO_{outlet})}{NO_{inlet}} \times 100$$

Immobilization of catalyst was carried out by the dip-coating method. Five grams of catalyst was first mixed with 100 mL deionized water to prepare slurry. Then the woven glass fabric (4 cm × 80 cm, pretreatment: 500 ºC, 1 h) was dip-coated with catalyst slurry. The loaded fabric was dried at 100 ºC for 1 h in an oven. This procedure was repeated three times and the final immobilized catalyst was then dried at 100 ºC for 24 h. The typical catalyst loading achieved by this approach was kept to be 0.5 g ± 10 %.

RESULTS AND DISCUSSION

Crystal structure: Fig. 1 shows the XRD pattern of Fe_2O_3-SnO_2 composites prepared at different molar ratios of Sn to Fe. The diffraction peaks at 2θ = 26.6, 33.8, 37.9 and 51.7º represented the (11 0), (1 0 1), (2 0 0) and (2 1 1) peaks of anatase SnO_2, respectively. The peaks at 2θ = 24.2º (0 1 2), 33.3º (1 0 4), 35.7º (1 1 0), 41.0º (1 1 3), 49.5º (024) and 64.2º (3 0 0) were attributed to the characteristic peaks of Fe_2O_3. The results demonstrated that when the molar ratios of Sn: Fe were 3:1 and 2:1 the characteristic peaks of the SnO_2 pattern were present; but when the molar ratios of Sn:Fe were 1:1 and 1:2 the characteristic peaks of the SnO_2 and Fe_2O_3 pattern were present. When the concentration of iron was increased (the molar ratio of Sn: Fe was 1:3), the peak intensity of Fe_2O_3 increased and the characteristic peaks of Fe_2O_3 became sharp and masked that of the SnO_2 peaks.

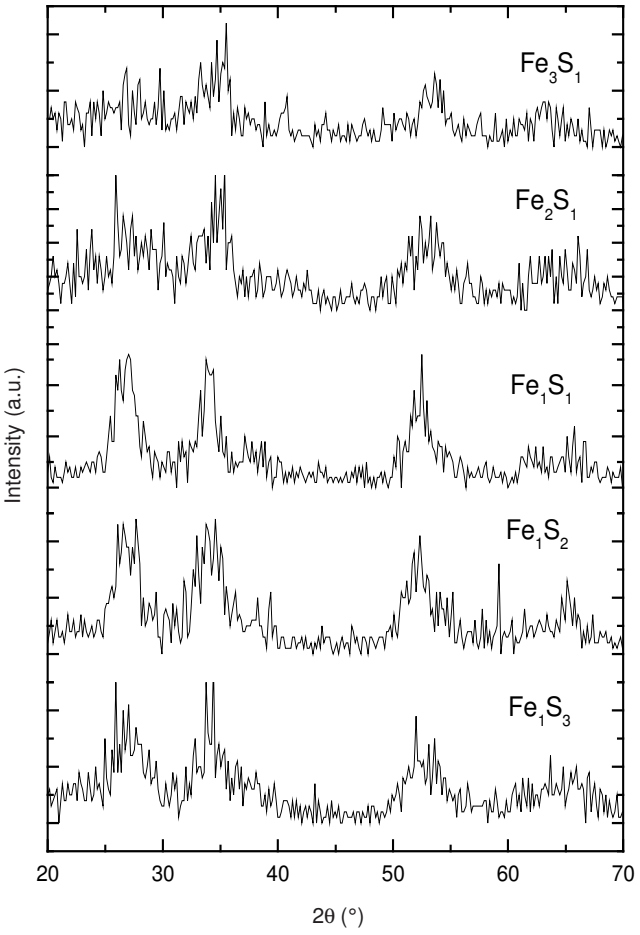

Fig. 1. XRD patterns of Fe_2O_3-SnO_2 composites with different molar ratios of Fe:Sn

UV-visible diffuse reflectance spectra (DRS UV-vis): Fig. 2 shows optical absorbance UV-visible diffuse reflectance spectra of Fe_2O_3-SnO_2 composites with different molar ratios of Fe:Sn. The results show that the absorption of Fe_1S_3 sample is *ca.* 410 nm. Increasing the molar ratio of Fe increasing the absorption in the visible region. It indicates that the Fe_2O_3-SnO_2 with high Fe molar ratio can be used as photocatalyst under visible light. The band gap energies (E_g) calculated on the basis of the corresponding absorption edges are shown in Fig. 2 and Table-1[23]. As shown in Table-1, the Fe_2O_3-SnO_2 composites calcined at 550 ºC for 5 h are the mixtures of Fe_2O_3 and SnO_2, so the band gap energies of the coupled Fe_2O_3-SnO_2 photocatalysts should originate from the overlapping of the corresponding Fe_2O_3 and SnO_2 components in the coupled oxides. It can be seen from Table-1 and Fig. 2 that the absorption edge of the coupled Fe_2O_3-SnO_2, or the band gap energy, changed with the Fe content. The band gap energy of the coupled Fe_2O_3-SnO_2 photocatalyst decreased with the increasing Fe content.

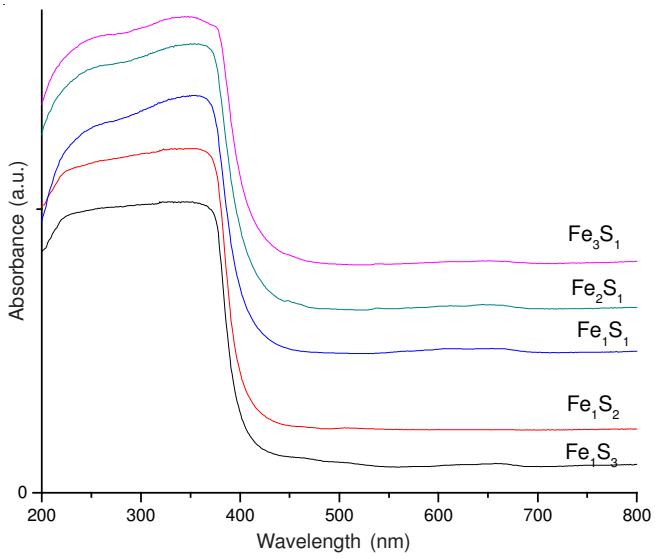

Fig. 2. UV-vis diffuse reflectance spectra of Fe_2O_3-SnO_2 composites with different molar ratios of Fe:Sn

TABLE-1
RELATIONSHIP OF COMPOSITION AND BAND GAP ENERGY

Sample	Band gap energy (eV)
Fe_1S_3	3.02
Fe_1S_2	2.90
Fe_1S_1	2.80
Fe_2S_1	2.60
Fe_3S_1	2.57

Surface area: The surface parameters of surface area and the data calculated from the *t*-plot were estimated by the low-temperature nitrogen adsorption at relative pressures (P/P_0) in the range of 0.05-0.9 and are given in Table-2. The N_2 adsorption isotherms for Fe_2O_3-SnO_2 nanoparticles (Fig. 3) are typical of type II. It could be seen that the surface areas were strongly dependent on the Fe content. It increased with increasing of Fe content.

Morphology: Fig. 4 shows TEM images taken for Fe_2O_3-SnO_2 nanoparticles. Powder samples were dispersed in ethanol

TABLE-2
TEXTURE PARAMETERS OF Fe_2O_3-SnO_2 NANOPARTICLES

Catalyst systems	S_{BET} (m^2/g)	S_t (m^2/g)	Total V_P (mL/g)	C_{BET}	r (Å)
Fe_1S_3	80.00	83.00	0.182	69.00	70.00
Fe_1S_2	95.00	94.00	0.195	74.00	52.00
Fe_1S_1	110.00	111.00	0.206	80.00	48.00
Fe_2S_1	120.00	121.00	0.218	88.00	45.00
Fe_3S_1	125.00	127.00	0.230	90.00	43.00

S_{BET}: BET Surface area. S_t surface area derived from $V_{l\text{-}t}$ plots. r^- mean pore radius. V_p total pore volume.

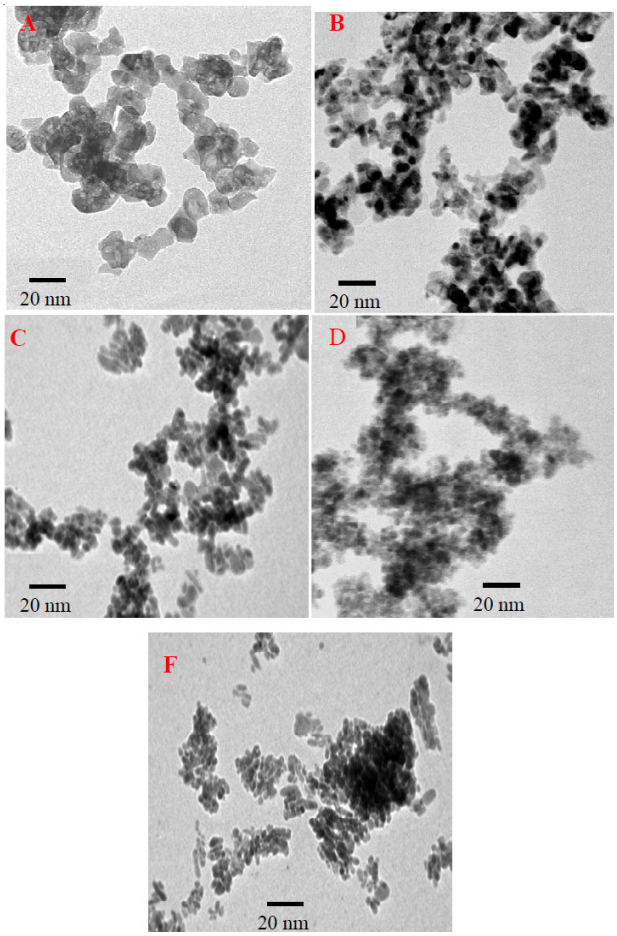

Fig. 3. TEM images of Fe_2O_3-SnO_2 composites with different molar ratios of Fe:Sn, where A = Fe_1S_3; B = Fe_1S_2; C = Fe_1S_1; D = Fe_2S_1; F = Fe_3S_1

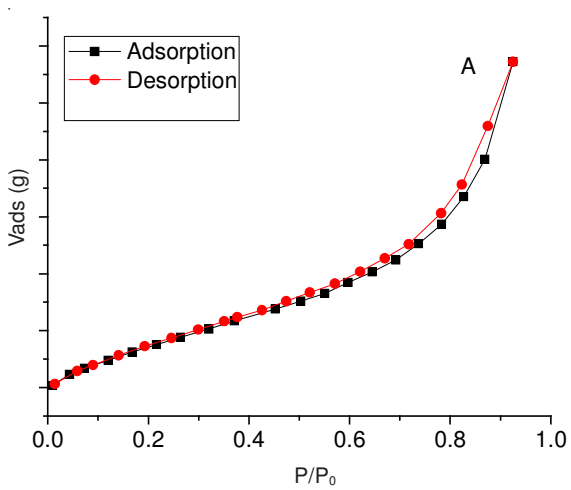

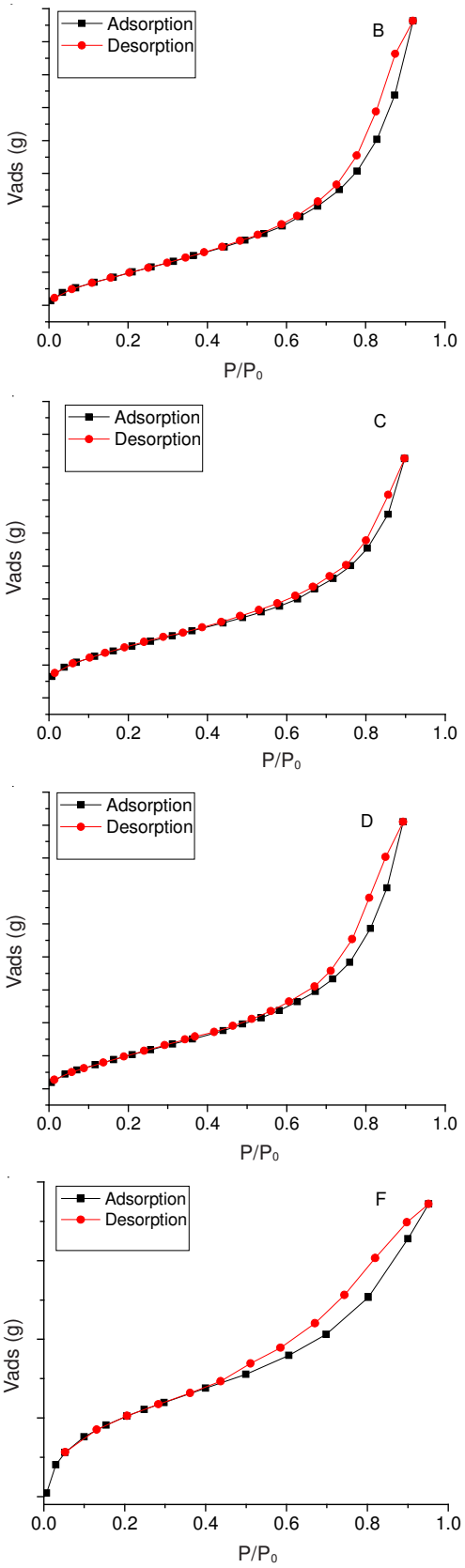

Fig. 4. N_2 sorption isotherms of Fe_2O_3-SnO_2 composites with different molar ratios of Fe:Sn, where A = Fe_1S_3; B = Fe_1S_2; C = Fe_1S_1; D = Fe_2S_1; F = Fe_3S_1

and sonicated in an ultrasonic bath for 15 min for TEM analysis. It is observed from Fig. 5 that SnO_2 grains have a spherical morphology with an average diameter of 16 nm for Fe_1S_3 and

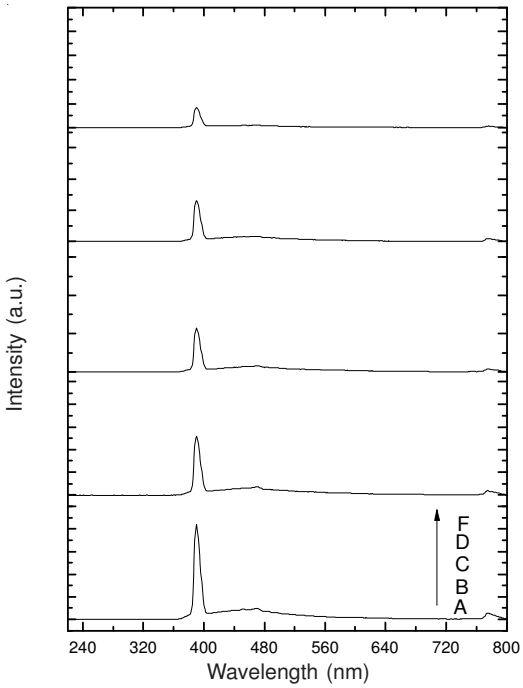

Fig. 5. Photoluminescence spectra of Fe_2O_3-SnO_2 composites with different molar ratios of Fe:Sn, where A = Fe_1S_3; B = Fe_1S_2; C = Fe_1S_1; D = Fe_2S_1; F = Fe_3S_1

13, 8, 6, 5 nm for Fe_1S_2, Fe_1S_1, Fe_2S_1 and Fe_3S_1 respectively, confirming the reduction in particle size of SnO_2 as a result of Fe_2O_3 doping in SnO_2.

Photoluminescence characteristics: Photoluminescence emission spectra have been used to study the transfer of the photogenerated electrons and holes and understand the separation and recombination of photogenerated charge carries[24]. In order to investigate the photoelectric properties of Fe_2O_3-SnO_2 nanoparticles, the photoluminescence spectra were detected for the different samples exited at 300 nm at room temperature (Fig. 5). The photoluminescence intensity greatly decreased with the increase of Fe content. Fe_2O_3 particles deposited on the surface could act as trapping sites to capture photogenerated electrons from SnO_2 conduction band, separating the photogenerated electron-hole pairs. Therefore, the recombination rate of photogenerated electrons and holes was retard, leading to reduction of photoluminescence signal decrease.

Photocatalytic activity studies of Fe_2O_3-SnO_2 composites

Behaviour of photocatalytic oxidation: Fig. 6 shows the variations of the conversion of NO with irradiation time over commercial SnO_2 and Fe_1S_1 catalyst in humidified environment. The results show that The NO conversion over SnO_2 decreased and approached a steady state after 5 h of irradiation. Similar results could be found in the literatures[25-27]. It is generally considered that the high initial conversion is the result of chemisorption[25]. It is indicated from Fig. 6 that the evolution of the activity *vs*. irradiation time for Fe_1S_1 is different from that for SnO_2. For Fe_1S_1 catalysts, the NO conversion increased with irradiation time and tended to be a constant value. With Fe_1S_1 catalyst, the minimum conversion (40 %) was observed at the beginning of reaction. After 14 h of irradiation, the conversion reached the maximum value of 75 %.

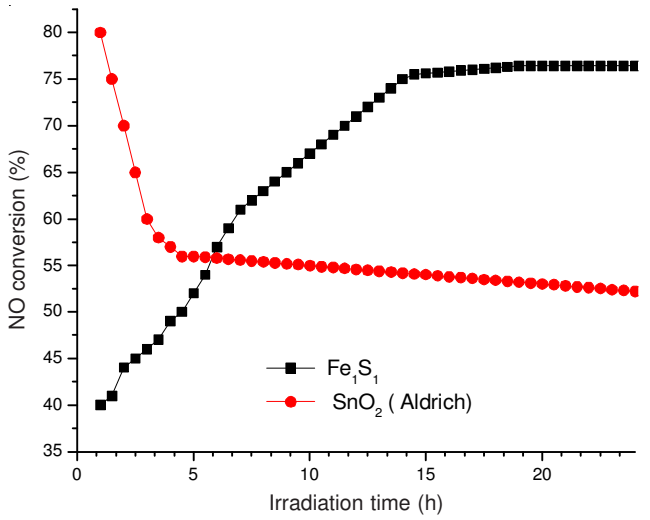

Fig. 6. Variations of NO conversion efficiency with irradiation time for nanoparticles SnO_2 Aldrich and Fe_1S_1

The compositions of hydroxyl groups on the surface of Fe_1S_1 under visible light irradiation could be possible reason. Under visible irradiation, $OH^•$ radicals could be produced from OH^- groups on the surface of SnO_2 oxidization by photo-generated holes.

$$SnO_2 + h\nu \rightarrow e^-_{CB} + h^+_{VB} \quad (1)$$

$$h^+_{VB} + H_2O_{ads} \rightarrow HO^-_{ads} + H^+ \quad (2)$$

$$h^+_{VB} + HO^-_{ads} \rightarrow HO^•_{ads} \quad (3)$$

$$e^-_{CB} + O_{2\,ads} \rightarrow O_2^{•-}{}_{ads} \quad (4)$$

$$NO + HO^•_{ads} \rightarrow HNO_2 \quad (5)$$

$$HNO_2 + HO_{ads} \rightarrow NO_2 + H_2O \quad (6)$$

$$NO_2 + HO^•_{ads} \rightarrow HNO_3 \quad (7)$$

$$NO + O_{2\,ads}{}^{•-} \rightarrow NO_3^- \quad (8)$$

Eqn. 3 reveals the formation of $OH^•$ radicals, which have been detected by ESR spin trapping[28-31]. Eqns. 5-7 indicate that $OH^•$ radicals play important roles in NO adsorption and oxidation process. Therefore, the enhanced photocatalytic oxidation of NO could be promoted by the increase in the concentration of surface OH^- groups. However, due to lack of the electron trapping sites like Fe species, the recombination rate between photogenerated holes and electrons was fast on SnO_2 and few holes could be utilized to oxidize surface oxygen atoms. Thus the increase of OH^- groups could not occur on SnO_2. For the photocatalytic oxidation of NO on SnO_2, $OH^•$ radicals participating in NO adsorption and reaction were mainly from adsorbed H_2O but not surface OH^- groups. During the initial state of the reaction, photogenerated electrons were transferred from SnO_2 conduction band to the Fe^{3+} and a portion of Fe^{3+} could be reduced. And the OH^- groups would be formed from SnO_2 surface oxygen atoms oxidation by photogenerated holes. $OH^•$ was scarily formed to participate in NO adsorption and oxidation reaction in the initial state, which resulted in the low conversion (Fig. 6). As the reaction going on, OH^- groups on the surface of SnO_2 could act as photogenerated holes trapping sites which is agree with photoluminescence results. It would let more $OH^•$ radicals to participate in the photocatalytic reaction and a rise in conversion could be observed (Fig. 6).

Photocatalytic activity: Fig. 7 shows the NO conversion efficiency on Fe_2O_3-SnO_2 nanoparticles after 14 h of irradiation

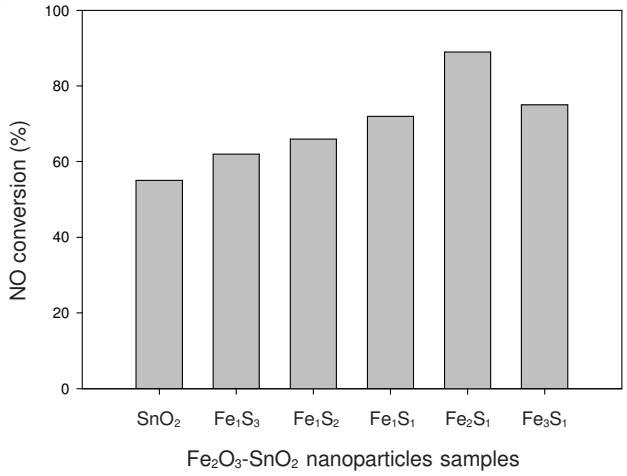

Fig. 7. Effect of Fe/Sn molar ratio on NO conversion %

with inlet NO concentration of 300 ppm. A series of Fe dopant contents, such as Fe_3S_1, Fe_2S_1, Fe_1S_1, Fe_1S_2 and Fe_1S_3, were chosen to investigate the relationship between the Fe contents and the photocatalytic activities of Fe_2O_3-SnO_2. It can be seen from Fig. 7 that the photocatalytic oxidation activity of NO greatly improves with the increase of molar ratio of Fe to Sn from 1:3 to 2:1 wt. %, then decreases with the further increasing molar ratio of Fe to Sn. Therefore, the optimum molar ratio of Fe to Sn was 2:1. The highest conversion occurred on Fe_2S_1, which was *ca.* 89 % which is higher than that with SnO_2 Aldrich nanoparticles (55 %). From the above-mentioned photoluminescence results (Fig. 5), it was indicated that the separation of the photogenerated electrons and holes was promoted after Fe doping. Moreover, the increase in the concentration of surface OH^- groups under bisible irradiation on Fe_2O_3-SnO_2 could result in more $OH^•$ radicals to participate in photocatalytic oxidization of NO. However, the enhancement of activity for Fe modification decreased when the Fe doping content was higher than 66.6 wt. %. It can be explained by the fact that the surface of SnO_2 was covered by too much Fe dopant so that it could not be irradiated efficiently, which reduced the apparent photo-quantum yield of photocatalytic process.

Fig. 8 shows the NO conversion efficiency on Fe_2S_1 and SnO_2 with different inlet concentration of NO. It can be shown in Fig. 8 that the photocatalytic oxidation efficiency of NO both decline with the increase of NO concentration. For SnO_2, the conversion of NO was 55 % when the inlet concentration was 85 ppm and decreased to 26 % when the inlet concentration reached 300 ppm. However, the photocatalytic activity of Fe_2S_1 performed well at higher concentration of NO. The conversion of NO (95 %) was *ca.* 1.72 times that of SnO_2 (55 %) at inlet NO concentration of 85 ppm, while the conversion (89 %) was *ca.* 3.42 times that of SnO_2 (26 %) at 300 ppm. The reason could be considered as the increasing adsorption sites of NO on surface of SnO_2 after Fe doping[30].

Conclusion

The novel visible-light-activated Fe_2O_3-SnO_2 nanocomposite photocatalyst was prepared by coprecipitation method. The characteristic patterns of XRD, BET, TEM, photoluminescence and UV-Vis-DRS displayed that the sample calcined

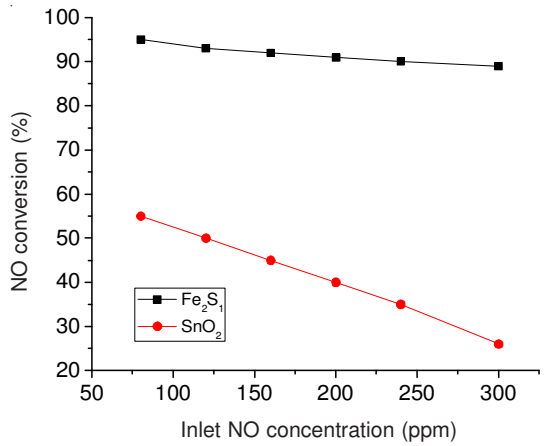

Fig. 8. Effect of NO concentration on NO conversion % of SnO_2 and Fe_2S_1

at 550 ºC for 5 h (the molar ratio of Fe to Sn is 2:1) has better crystallization, smaller crystal size and stronger response to visible light. The experimental results showed that the optimum Fe dopant content was the molar ratio of Fe to Sn is 2:1. With the molar ratio of Fe to Sn is 2:1, the concentration of NO could reach 89 % with inlet NO concentration of 300 ppm, which was 89 % higher than that of SnO_2. Full characterizations of Fe_2O_3-SnO_2 were also conducted to investigate the relationship between the physicochemical properties and photocatalytic activity. Photoluminescence spectra identified that the doping of Fe on SnO_2 could inhibit the recombination of photogenerated electrons and holes. In a sense, this work may provide new insights into the development of novel sunlight photocatalysts.

REFERENCES

1. A. Farrell, *Energy Policy*, **29**, 1061 (2001).
2. T. Castro, S. Madronich, S. Rivale, A. Muhlia and B. Mar, *Atmos. Environ.*, **35**, 1765 (2001).
3. C.D. Cooper and F.C. Alley, Air Pollution Control: A Design Approach, Waveland Press, Prospect Heights, IL (1994).
4. X.L. Tang, J.M. Hao,W.G. Xu and J.H. Li, *Catal. Commun.*, **8**, 329 (2007).
5. J.M. Beer, *Prog. Energy Combust. Sci.*, **26**, 301 (2000).
6. A.M. Efstathiou and K. Fliatoura, *Appl. Catal. B: Environ.*, **6**, 35 (1995).
7. Y.S. Mok, *Chem. Eng. J.*, **118**, 63 (2006).
8. Y.G. Adewuyi and S.O. Owusu, *Ind. Eng. Chem. Res.*, **42**, 4084 (2003).
9. M. Rodriguez, V. Sarria, S. Esplugas and C. Pulgarin, *J. Photochem. Photobiol. A Chem.*, **151**, 129 (2002).
10. M.S. Siboni, M.-T. Samadi, J.-K. Yang and S.-M. Lee, *Desalin. Water Treat.*, **40**, 77 (2012).
11. N.M. Mahmoodi and M. Arami, *Desalin. Water Treat.*, **1**, 312 (2009).
12. Y. Nakaoka, H. Katsumata, S. Kaneco, T. Suzuki and K. Ohta, *Desalin. Water Treat.*, **13**, 427 (2010).
13. M. Nasr-Esfahani, A. Khakifirooz, N. Tavakoli and M.H. Soleimani, *Desalin. Water Treat.*, 21, 202 (2010).
14. B.H. Hameed, U.G. Akpan and Keng Poh Wee, *Desalin. Water Treat.* **27**, 204 (2011).
15. B. Kosowska, S. Mozia, A.W. Morawski, B. Grzmil and M. Janus, *Sol. Energy Mater. Sol. Cells*, **88**, 269 (2005).
16. S. Kohtani, M. Tomohiro, K. Tokumura and R. Nakagaki, *Appl. Catal. B: Environ.*, **58**, 265 (2005).
17. S. Kumar, A.G. Fedorov and J.L. Gole, *Appl. Catal. B: Environ.*, **57**, 93 (2005).
18. C. Wang, J. Zhao, X.Wang, B. Mai, G. Sheng, P. Peng and J. Fu, *Appl. Catal. B: Environ.*, **39**, 269 (2002).
19. B.S. Liu, X.J. Zhao, N.Z. Zhang, Q.N. Zhao, X. He and J.Y. Feng, *Surf. Sci.*, **595**, 203 (2005).
20. X.Z. Li, F.B. Li, C.L. Yang and W.K. Ge, *J. Photochem. Photobiol. A Chem.*, **141**, 209 (2001).
21. C. Wang, X.M. Wang, B.Q. Xu, J.C. Zhao, B.X. Mai, P.A. Peng, G.Y. Sheng, J.M. Fu, *J. Photochem. Photobiol. A Chem.*, **168**, 47 (2004).
22. X.D. Yu, Q.Y. Wu, S.C. Jiang and Y.H. Guo, *Mater. Charact.*, **57**, 333 (2006).
23. A. Hagfeldt and M. Gratzel, *Chem. Rev.*, **95**, 49 (1995).
24. W.F. Zhang, M.S. Zhang, Z. Yin and Q. Chen, *Appl. Phys. B*, **70**, 261 (2000).
25. S. Devahasdin, C. Fan Jr., K. Li and D.H. Chen, *J. Photochem. Photobiol. A*, **156**, 161 (2003).
26. H.Q. Wang, Z.B. Wu, W.R. Zhao and B.H. Guan, *Chemosphere*, **66**, 185 (2007).
27. Z.B. Wu, H.Q. Wang, Y. Liu and Z.L. Gu, *J. Hazard. Mater.*, **151**, 17 (2008).
28. T.A. Egerton and I.R. Tooley, *J. Phys. Chem. B*, **108**, 5066 (2004).
29. T. Hirakawa, H. Kominami, B. Ohtani and Y. Nosaka, *J. Phys. Chem. B*, **105**, 6993 (2001).
30. T. Ohno, K. Sarukawa, K. Tokieda and M. Matsumura, *J. Catal.*, **203**, 82 (2001).
31. S. Roy, M.S. Hegde, N. Ravishankar and G. Madras, *J. Phys. Chem. C*, **111**, 8153 (2007).